GEOPHYSICS, VOL. 77, NO. 3 (MAY-JUNE 2012); P. WA157–WA168, 9 FIGS.
10.1190/GEO2011-0253.1

Modeling squirt dispersion and attenuation in fluid-saturated rocks using pressure dependency of dry ultrasonic velocities

Osni Bastos de Paula[1], Marina Pervukhina[2], Dina Makarynska[3], and Boris Gurevich[4]

ABSTRACT

Modeling dispersion and attenuation of elastic waves in fluid-saturated rocks due to squirt flow requires the knowledge of a number of geometrical parameters of the pore space, in particular, the characteristic aspect ratio of the pores. These parameters are usually inferred by fitting measurements on saturated rocks to model predictions. To eliminate such fitting and thus make the model more predictive, we propose to recover the geometrical parameters of the pore space from the pressure dependency of elastic moduli on dry samples. Our analysis showed that the pressure dependency of elastic properties of rocks (and their deviation from Gassmann's prediction) at ultrasonic frequencies is controlled by the squirt flow between equant, stiff, and so-called intermediate pores (with aspect ratios between 10^{-3}–2×10^{-1}). Such intermediate porosity is expected to close at confining pressures of between 200 and 2000 MPa, and thus cannot be directly obtained from ultrasonic experiments performed at pressures below 50 MPa. However, the presence of this intermediate porosity is inferred from the significant linear trend in the pressure dependency of elastic properties of the dry rock and the difference between the bulk modulus of the dry rock computed for spherical pores and the measured modulus at 50 MPa. Moreover, we can infer the magnitude of the intermediate porosity and its characteristic aspect ratio. Substituting these parameters into the squirt model, we have computed elastic moduli and velocities of the water-saturated rock and compared these predictions against laboratory measurements of these velocities. The agreement is good for a number of clean sandstones, but not unexpectedly worse for a broad range of shaley sandstones. Our predictions showed that dispersion and attenuation caused by the squirt flow between compliant and stiff pores may occur in the seismic frequency band. Confirmation of this prediction requires laboratory measurements of elastic properties at these frequencies.

INTRODUCTION

Understanding dispersion and attenuation of elastic waves in rocks is important for consistent analysis of seismic, borehole acoustic, and ultrasonic data. A major cause of elastic wave dispersion and attenuation in fluid-saturated rocks is the so-called squirt flow, that is, local (pore-scale) wave-induced flow of the pore fluid between pores of different shapes and orientations (Mavko and Nur, 1975, 1979; Jones, 1986). When an elastic wave propagates through a fluid-saturated medium, relatively compliant pores are deformed to a greater degree than the relatively stiff ones. This difference creates local pressure gradients within the fluid phase, resulting in fluid flow and corresponding energy dissipation that continues until the pore pressure is equilibrated.

Over the last 40 years a number of theoretical models of squirt dispersion and attenuation have been proposed with different assumptions concerning the distribution of pore shapes and orientations. Most theoretical models of squirt-flow attenuation are based on the analysis of aspect ratio distributions (O'Connell and Budiansky, 1977; Mavko and Nur, 1979; Palmer and Traviolia, 1980); a comprehensive review of these earlier studies is given

Manuscript received by the Editor 11 July 2011; revised manuscript received 31 October 2011; published online 23 April 2012.
[1]PETROBRAS/E&P-EXP/GEO/ES, Gerência de Estratigrafia e Sedimentologia, Rio de Janeiro, Brazil; Curtin University of Technology, Department of Exploration Geophysics, Perth, Australia. E-mail: osnidepaula@petrobras.com.br.
[2]CSIRO Earth Sciences and Resource Engineering, ARRC, Perth, Australia. E-mail: marina.pervukhina@csiro.au.
[3]Curtin University of Technology, Department of Exploration Geophysics, Perth, Australia. E-mail: dgmakarynska@ovi.com.
[4]CSIRO Earth Sciences and Resource Engineering, ARRC, Perth, Australia; Curtin University of Technology, Department of Geophysics, Perth, Australia. E-mail: b.gurevich@curtin.edu.au.

by Jones (1986). An alternative approach is based on the recognition that the pore space of many rocks has a binary structure (Walsh, 1965; Mavko and Jizba, 1991; Shapiro, 2003): relatively stiff pores, which form most of the pore space, and relatively compliant (or soft) pores, which mostly contribute for the pressure dependency of the elastic moduli (Murphy et al., 1986; Dvorkin et al., 1995; Chapman et al., 2002; Gurevich et al., 2010). In these models, the magnitude of dispersion is related to the amount of soft porosity, while the characteristic frequency of the squirt dispersion is related to the degree of compliance of the soft pores (often expressed as the characteristic aspect ratio of these soft pores). This characteristic compliance or aspect ratio cannot be measured directly and often is taken to be an adjustable parameter that can be obtained by fitting of the model to experimental data (such as the dispersion curve measured in the laboratory). The existence of an adjustable parameter that cannot be independently measured is a weakness of all squirt models, as it impedes independent verification of these models.

Mavko and Jizba (1991) showed that the magnitude of the squirt dispersion can be related directly to the pressure dependency of the elastic dry moduli of the dry rock. At the same time, this pressure dependency also defines the characteristic compliance (or aspect ratio) of the soft pores (Walsh, 1965; Shapiro, 2003). By estimating the characteristic pore compliance from the rock's pressure dependency, we can eliminate the adjustable parameter in the squirt model. The purpose of this paper is to establish such a workflow, and to test it against laboratory measurements.

The paper is organized as follows. First, we briefly recall a simple theoretical model of squirt-flow dispersion (as proposed by Gurevich et al., 2010), as well as a model of stress dependency of elastic moduli of dry rocks (Shapiro, 2003). We then propose the new concept of intermediate porosity to describe the pressure dependency of elastic moduli for pressures above 50 MPa. The next section outlines the workflow employed to obtain the geometrical pore space parameters from pressure dependency of the elastic moduli, and to predict the dispersion and attenuation in fluid-saturated rocks using the squirt model. This is followed by laboratory data examples where the predictions for water-saturated rocks are compared with the ultrasonic measurements.

THEORETICAL MODELS

A squirt model

Squirt is a phenomenon of wave-induced pressure relaxation and fluid flow between pores of different shapes and/or orientations, and, more specifically, between relatively compliant and relatively stiff pores. Mavko and Jizba (1991) showed that at high frequencies

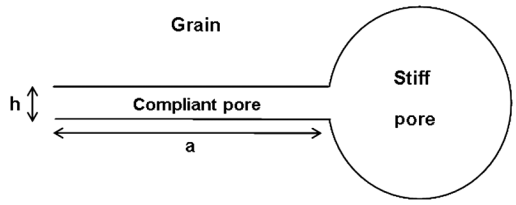

Figure 1. Cross section of the idealized geometry of compliant and stiff pores (Murphy et al., 1986). A disc-shaped compliant pore forms a gap between two grains and its edge opens into a toroidal stiff pore.

(such that the fluid pressure has no time to equilibrate between pores of different stiffnesses/orientations), the effect of the squirt phenomenon on elastic properties is relatively independent of the assumptions about pore geometries. For such high frequencies, the squirt effect can be modeled via a so-called *modified frame* concept. Modified frame refers to the state of the rock in which the stiff pores are dry while the compliant pores are saturated with a fluid. Mavko and Jizba (1991) showed that in the high-frequency limit, pressure dependency of the bulk and shear moduli $K_{\mathrm{mf}}(P)$ and $\mu_{\mathrm{mf}}(P)$ of the modified frame can be expressed as

$$\frac{1}{K_{\mathrm{mf}}(P)} = \frac{1}{K_h} + \left(\frac{1}{K_f} - \frac{1}{K_g}\right)\phi_c(P) \tag{1}$$

$$\frac{1}{\mu_{\mathrm{uf}}(P)} = \frac{1}{\mu_d(P)} + \frac{4}{15}\left(\frac{1}{K_{\mathrm{mf}}(P)} - \frac{1}{K_d(P)}\right) \tag{2}$$

where $\phi_c(P)$ is the compliant porosity as a function of effective pressure P, $K_d(P)$ and $\mu_d(P)$ are bulk and shear moduli of the dry frame, K_h is the dry bulk modulus in the high-pressure-limit (when all the compliant porosity is closed), and K_g is the bulk modulus of the solid grain material. Conversely, in the low-frequency limit, the pore pressure has ample time to equilibrate between stiff and compliant pores, and thus, the bulk and shear moduli of the modified frame are equal to those of the completely dry frame.

At intermediate frequencies, the fluid pressure would equilibrate partially and elastic properties would become dependent not only on pressure but also on frequency and geometry of the pore space. Murphy et al. (1986) proposed to represent the geometry of the compliant pores as flat slabs connecting stiffer pores (Figure 1). For granular rocks such as sandstones, stiff pores represent intergranular pores defined by the grain packing, while the flat slabs represent gaps at contacts between adjacent grains. Using the geometrical configuration proposed by Murphy et al. (1986), Gurevich et al. (2010) showed that the frequency dependent bulk and shear moduli of the modified frame are given by the following analytical expressions

$$\frac{1}{K_{\mathrm{mf}}(P,\omega)} = \frac{1}{K_h} + \frac{1}{\frac{1}{\frac{1}{K_d(P)} - \frac{1}{K_h}} + \frac{3i\omega\eta}{8\phi_c(P)\alpha_c^2}} \tag{3}$$

and

$$\frac{1}{\mu_{\mathrm{mf}}(P,\omega)} = \frac{1}{\mu_d(P)} - \frac{4}{15}\left(\frac{1}{K_d(P)} - \frac{1}{K_{\mathrm{mf}}(P,\omega)}\right). \tag{4}$$

In equations 3 and 4, ω is the angular frequency of the wave, η is the dynamic viscosity of the pore fluid, and α_c is the aspect ratio of the intergranular gap (thickness over diameter). Equation 3 has a restriction that the fluid modulus must satisfy the condition

$$K_f \gg 8\phi_c\left(\frac{1}{K_d} - \frac{1}{K_h}\right)^{-1}. \tag{5}$$

This means that the fluid modulus should not be too small, i.e., the fluid inside the crack must be a liquid. The frequency dependent

bulk modulus of the rock fully saturated with the fluid K_s can be obtained from the frequency dependent modulus K_{mf} of the modified frame using Gassmann's (1951) equation

$$\frac{1}{K_s(P,\omega)} = \frac{1}{K_g} + \frac{\phi\left(\frac{1}{K_f} - \frac{1}{K_g}\right)}{1 + \phi\left(\frac{1}{K_f} - \frac{1}{K_g}\right)/\left(\frac{1}{K_{\mathrm{mf}}(P,\omega)} - \frac{1}{K_g}\right)}, \quad (6)$$

where ϕ is the total porosity. The saturated shear modulus μ_s is equal to the shear modulus of the modified frame μ_{mf}

$$\mu_s = \mu_{\mathrm{mf}}. \quad (7)$$

The saturated moduli K_s and μ_s computed with equations 3, 4, 6, and 7 are consistent with Gassmann's equation in the low-frequency limit and with Mavko-Jizba (1991) equations 1 and 2 in the high-frequency limit. Between these limits, the moduli are complex and frequency dependent, and thus the corresponding elastic waves exhibit attenuation and dispersion. Furthermore, at frequencies where viscoinertial relaxation becomes important, these equations can be combined with Biot's (1962) equations of poroelasticity to account for squirt and local and Biot's global flow dissipation mechanisms (Carcione and Gurevich, 2011).

Stress dependency of the elastic parameters of a dry rock

The squirt equations 3 and 4 require knowledge of the pressure dependence of the dry bulk and shear moduli and of what fraction of the total porosity is compliant porosity. Commonly, the dependence the dry rock velocity on stress is described by a combination of linear and exponential terms (Eberhart-Phillips et al., 1989; Zimmerman, 1991)

$$V(P) = A + KP - Be^{-DP}, \quad (8)$$

where V is velocity (of P or S waves) in km/s, P is confining pressure in kbars, A, K, B, and D are fitting parameters that provide the best agreement with the measured data. A number of authors explained the exponential term in equation 8 by the presence and closure of pores with a wide spectrum of aspect ratios (e.g., Zimmerman, 1991; Tod, 2002). However, Shapiro (2003) shows that the experimentally observed stress dependency (equations 8) also can be explained by the presence (and closure) of only two types of pores, namely, stiff porosity ϕ_s, which decreases linearly with the increasing confining stress, and soft or compliant porosity ϕ_c, which is defined as the difference between the total porosity ϕ minus stiff porosity ($\phi_c = \phi - \phi_s$) (see Walsh, 1965; Mavko and Jizba, 1991). Shapiro (2003) shows that if the pore space consists of stiff and compliant porosities so defined, then the stress dependency of its dry compressibility $C_d = 1/K_d$ can be written as

$$C_d(P) = C_{ds0}[1 - \theta_s \Delta\phi_s(P) + \theta_c \phi_c(P)], \quad (9)$$

where $C_{ds0} = 1/K_h$ is the drained compressibility of a hypothetical rock with the compliant porosity closed and stiff porosity equal to $\phi_{s0} = \phi_s(0)$, θ_s and θ_c are the pressure sensitivity coefficients for stiff and compliant porosity, respectively, and $\Delta\phi_s(P) = \phi_s(P) - \phi_{s0}$. Shapiro (2003) further showed that the pressure dependencies of the stiff and compliant porosities can be expressed by

$$\phi_s = \phi_{s0} - P(C_{ds0} - C_g) \quad (10)$$

and

$$\phi_c = \phi_{c0} e^{-\theta_c C_{ds0} P}. \quad (11)$$

where $\phi_{s0} = \phi_{s0}(0)$ and $\phi_{c0} = \phi_c(0)$ are values of the stiff and compliant porosity in the unstressed rock, and $C_g = 1/K_g$ is the grain compressibility. The linear relationship nine between the rock compressibility obtained from ultrasonic velocities, and compliant porosity obtained from strain measurements was demonstrated for a number of sandstones by Pervukhina et al. (2010). The theoretically predicted relation that explicitly expresses the stress dependency of the dry elastic compressibility can then be obtained by combining equations 9–11 as follows

$$C_d(P) = C_{ds0}[1 - \theta_s(C_{ds0} - C_g)P + \theta_c \phi_{c0} e^{-\theta_c C_{ds0} P}]. \quad (12)$$

The relationship nine between the drained compressibility and compliant porosity can be used in combination with the squirt equations 3 and 4 to obtain an explicit dependency of the elastic moduli of the saturated rock on pressure and frequency. Furthermore, the stress sensitivity coefficient θ_c for compliant porosity can be related to the characteristic aspect ratio α_c of the compliant pores by the equation for bulk modulus of an elastic medium with a dilute concentration of ellipsoidal cavities (Christensen, 2005; Mavko, et al., 1988; Kuster and Toksöz, 1974)

$$\theta_c = \frac{K_h(3K_h + 4\mu_h)}{\pi\alpha_c\mu_h(3K_h + \mu_h)}. \quad (13)$$

The use of the dilute concentration model is justified by the linear relationship nine between the sandstone compressibility and compliant porosity (Pervukhina et al., 2010). In equation 13, K_h and μ_h denote elastic moduli of the rock without open compliant pores, and with the stiff porosity equal to ϕ_{s0}. Thus, equations 9 and 11 imply that the exponential decrease of the elastic moduli with the increase of confining pressure can be achieved by the progressive closure of compliant pores of a (approximately) constant aspect ratio, rather than by the change of the aspect ratio. However, the overall pore shape distribution does change because the compliant porosity changes with pressure much more rapidly than the stiff porosity. The values of the coefficient θ_c obtained by fitting equations 9–11 to experimental pressure dependencies of the elastic moduli yield aspect ratios in the range 0.03×10^{-4}–0.3×10^{-4}. Note also that roughly speaking, coefficient θ_c is on the order of α_c^{-1}; in other words, the characteristic crack closing pressure is

$$P_c = K_h/\theta_c = \alpha_c K_h \quad (14)$$

MODERATELY STIFF (INTERMEDIATE) POROSITY

The concept of intermediate porosity

In his analysis of the contribution of the stiff porosity term in equation 9, Shapiro (2003) assumes that the stiff pores have aspect ratios of order one (so-called equant pores, Thomsen, 1995), and

concludes that the contribution of the deformation of the stiff porosity is small compared to that of the compliant porosity, and thus can be neglected. However, experimental studies (Eberhart-Phillips et al., 1989; Vernik and Hammam, 2009; Gurevich et al., 2010) show that in many cases, the contribution of the stiff porosity term (that is, the term that varies linearly with pressure in the pressure range between 0 and 50 MPa) is significant. This implies that the stress sensitivity coefficient θ_s for stiff porosity is significantly larger than that for spherical or equant pores. In other words, experimental data suggest that in addition to equant pores, the stiff porosity contains pores with aspect ratios greater than 0.3×10^{-1} but much less than one. In analogy with equations 12 and 13, such porosity would decrease exponentially with the increasing pressure and close approximately at $P_s = \alpha_s K_e$, where K_e is the bulk modulus of a rock

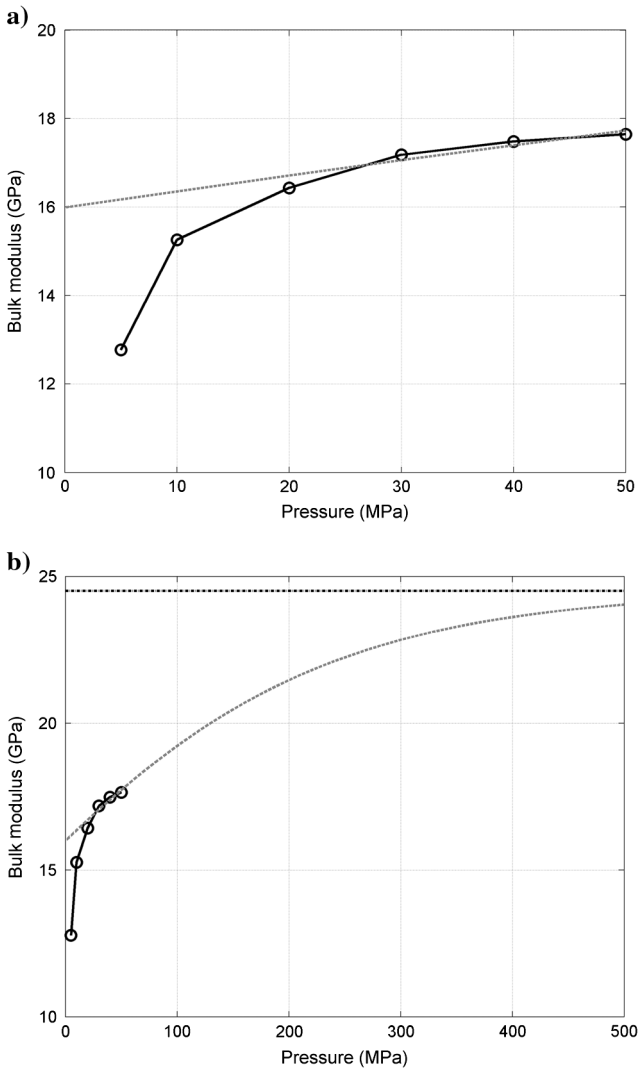

Figure 2. Dry bulk modulus stress dependency for a sample of St. Peter sandstone: (a) up to pressure of 50 MPa; (b) above 50 MPa. The bulk moduli calculated from the ultrasonic velocity measurements and interpolated to the intermediate pressures are shown by open circles and solid line, respectively. Variation of the bulk modulus predicted for the higher pressures and caused by closing of the intermediate porosity is marked by a dashed line. The dashed-dotted line indicates the bulk modulus of the "Swiss cheese" limit for the sandstone.

with only equant pores present (so-called Swiss-cheese rock). The modulus K_e is usually on the order of (but somewhat smaller than) the grain bulk modulus K_g. Thus, for a rock such as sandstone, P_s would be on the order of 200–2000 MPa. This is much larger than the maximum pressure typically applied in ultrasonic pressure cell experiments, and the exponential decrease of such porosity with confining pressure would look like a linear decrease in the pressure range, say, from zero to 40 MPa.

The above analysis suggests that it is reasonable to divide the stiff porosity ϕ_s into two parts: the equant porosity ϕ_e with characteristic aspect ratio close to one, and moderately stiff or intermediate porosity ϕ_m with a characteristic aspect ratio in the range 10^{-3}–2×10^{-1}

$$\phi_s = \phi_e + \phi_m, \tag{15}$$

or, for the total porosity ϕ

$$\phi = \phi_e + \phi_m + \phi_c. \tag{16}$$

Stress dependency of dry moduli in the presence of intermediate porosity

By definition, the compressibility of the intermediate porosity is much higher than the compressibility of the equant porosity. Thus, the intermediate porosity will exhibit an exponential decay with increasing pressure, similar to the compliant porosity but at much higher confining pressures

$$\phi_m = \phi_{m0} e^{-\theta_m C_e P}, \tag{17}$$

where ϕ_m is porosity of the intermediate pores, ϕ_{m0} is the intermediate porosity at zero confining stress, θ_m is stress sensitivity of these pores and $C_e = 1/K_e$ is the compressibility of the dry rock with equant pores only.

Closure of the intermediate porosity at such stresses will affect the compressibility of the rock in a similar way as closing of compliant pores affects compressibility at 0–50 MPa and its effect can be described by a similar equation

$$C_{ds}(P) = C_e[1 + \theta_m \phi_m(P)] \tag{18}$$

or

$$C_{ds}(P) = C_e[1 + \theta_m \phi_{m0} e^{-\theta_m C_e P}]. \tag{19}$$

In equations 18 and 19, C_{ds} is the compressibility of a hypothetic rock without the compliant porosity (that is, only with stiff porosity $\phi_s = \phi_e + \phi_m$ open). Furthermore, the effect of the deformation of equant porosity is neglected. For large pressures where the compliant porosity is closed (above 50–100 MPa), $C_{ds}(P) = C_d(P)$. The variation of the dry compressibility due to the combined effect of compliant and intermediate porosity can be written as

$$C_d(P) = C_e[1 + \theta_m \phi_{m0} e^{-\theta_m C_e P} + (1 + \phi_{m0})\theta_c \phi_{c0} e^{-\theta_c C_{ds0} P}]. \tag{20}$$

The stress dependency of the bulk modulus of typical reservoir sandstone is shown in Figure 2a. Open circles at stresses of 5–50 MPa are the bulk moduli calculated from the experimentally

measured ultrasonic velocities of St. Peter sandstone (Han et al., 1986) and the solid line shows the approximation of the moduli with equations 9–11. The dashed-dotted horizontal line shows the bulk modulus of the rock in the high-pressure limit, where all intermediate porosity is closed ("Swiss-cheese" limit). We calculate this limit using the coherent potential approximation (CPA) effective medium model for spherical pores (Berryman, 1980). Instead of CPA, differential effective medium (DEM) approximation (Cleary et al., 1980; Norris, 1985; Zimmerman, 1991) could be used. For porosities below, say, 0.25 and aspect ratios of order one, these models give similar results, but for sandstones with higher porosities CPA is more adequate (Berge et al., 1993, 1995). The dashed line is the fit of C_{ds} using equation 19, which shows the effect of the closure of the intermediate porosity. Figure 2b shows the effect of the compliant and intermediate porosity on the bulk modulus in the wider range of confining stresses of 5–500 MPa for the same sample. One can see that at low stresses, the effect of the closure of the intermediate porosity is almost linear.

The importance of the intermediate porosity can be demonstrated by comparing the bulk moduli measured at the highest confining stress in pressure cell experiments against estimates of the bulk moduli in the "Swiss cheese" limit, in which all porosity consists of equant pores. Indeed, typical values of the constant D in equation 8 are above 0.03 MPa^{-1} (Eberhart-Phillips et al., 1989; Shapiro, 2003), which means that at pressures above about 50 MPa we can assume the compliant porosity to be closed. Thus, if all the stiff porosity consisted of equant pores (no intermediate porosity), the bulk modulus measured at the pressure of 50 MPa would be equal to that computed for spherical pores. However, the analysis of the St. Peter sandstone (Figure 2) shows an obvious difference of about 7 GPa between the measured bulk modulus at 50 MPa, and the predicted bulk modulus of the rock at the Swiss-cheese limit,K_e computed using CPA.

Figure 3a is a plot of dry bulk modulus K_{50} at $P = 50$ MPa against the "Swiss-cheese" limit K_e for 66 dry sandstones with different mineralogy and clay content from different depths and locations as obtained from ultrasonic measurements of Han et al. (1986). The "Swiss cheese" limit K_e is computed for each sandstone by using CPA for spherical pores. The grain bulk and shear moduli K_g and μ_g used in CPA are obtained using the linear empirical fits for compressional and shear velocities (in km/s) of shaley sandstones (Han et al., 1986)

$$V_{\text{P}g} = 5.59 - 2.18F_c \tag{21}$$

and

$$V_{\text{S}g} = 3.52 - 1.89F_c \tag{22}$$

where F_c is the clay content. Figure 3a shows that for all 66 sandstones, the modulus K_{50} is much lower than the K_e with the difference ranging 5 to 15 GPa. We explain this difference by the presence of the intermediate porosity that is still open at the stress of 50 MPa.

The mismatch between the experimentally measured elastic moduli at 50 MPa and estimated effective elastic moduli of Swiss cheese rock with stiff porosity only cannot be explained with presence of stiff pores with aspect ratios smaller than unity. Figure 3b shows variations of the normalized bulk elastic moduli with porosity for all the sandstones. CPA predicted variations of the effective bulk moduli for the inclusions with aspect ratios of 0.01–1.0 are shown by lines. The difference between elastic moduli of rocks with the same porosity and aspect ratios of 1.0 and 0.5 is very small. The measured elastic moduli exhibit the same trend with the porosity increase as CPA predictions for aspect ratios of 0.2 and smaller. We consider pores with such aspect ratio as intermediate porosity. The normalized elastic moduli vs. porosity trends, which correspond to CPA predictions for the pores with aspect ratios smaller than 0.2, can be considered as an independent verification of the existence of the intermediate porosity.

Once existence of intermediate pores is established, we need to check whether all the stiff porosity can be considered as intermediate with a single effective aspect ratio less than 0.2 (without any equant porosity). If there is no equant porosity, then in equations 19 $C_e = 1/K_g$ and $\phi_{m0} = \phi_{s0} \simeq \phi$. Then linearization of equations 19 for small pressures gives

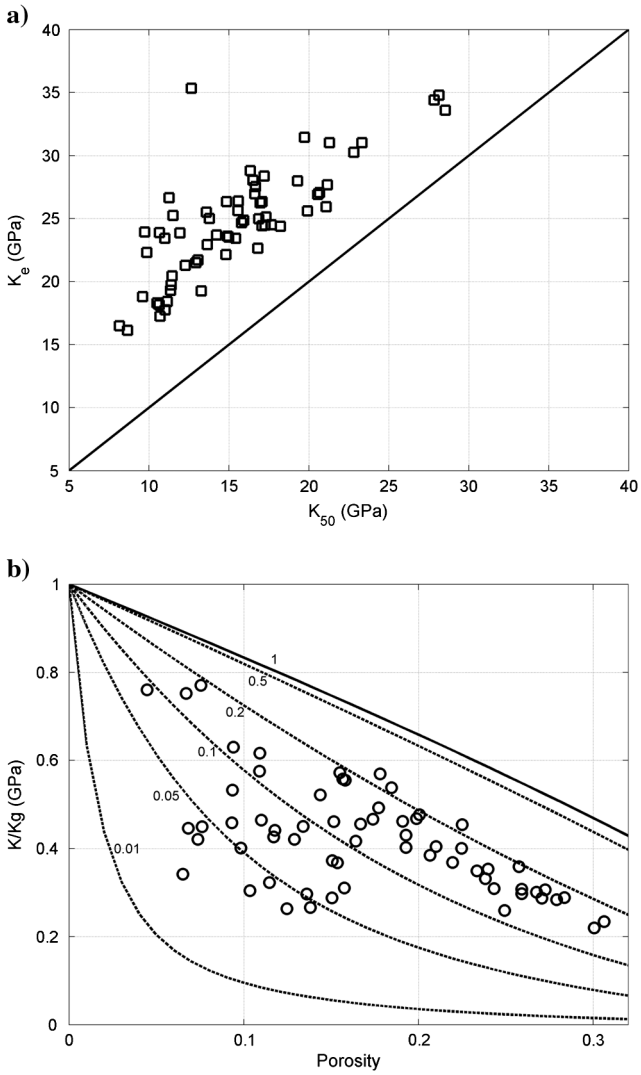

Figure 3. Bulk moduli of sandstones calculated from experimentally measured ultrasonic velocities (Han et al., 1986). (a) Dry experimentally measured bulk moduli, K_{50}, at 50 MPa versus dry bulk moduli, K_e, of the same sandstones at the hypothetic "Swiss cheese limit." (b) K_{50} normalized by grain bulk modulus versus porosity in comparison with the CPA prediction.

$$C_{ds} = C_g[1 + \phi_{s0}\theta_m - \phi_{s0}\theta_m^2 C_g P]. \quad (23)$$

Thus the stress dependency of bulk modulus can be written as

$$K_{ds} = K_g[1 - \phi_{s0}\theta_m + \phi_{s0}\theta_m^2 C_g P]. \quad (24)$$

Analysis of ultrasonic data for different classes of rocks shows that the stress sensitivity coefficients are similar for the bulk and shear moduli (Eberhart-Phillips et al., 1989; Takei, 2002; Shapiro, 2003). Thus, the linearized velocity-pressure dependency can be approximately written as

$$\begin{aligned} V_P &= V_g[1 - \phi_{s0}\theta_m/2 + \phi_{s0}\theta_m^2 C_g P/2] \\ &= V_g[1 - \phi_{s0}\theta_m/2] + V_g\phi_{s0}\theta_m^2 C_g P/2. \end{aligned} \quad (25)$$

Comparison of equations 25 with equation 8 without the exponential term gives the following approximate expression for coefficient K in equation 8

$$K = \frac{1}{2}\phi_{s0}\theta_m^2 V_g/K_g. \quad (26)$$

For a typical sandstone, taking $\phi = 0.2$, $V_g = 5$ km/s, $\theta_m = 3$ (assuming an aspect ratio of 0.2; Takei, 2002) and $K_g = 40$ GPa = 400 kbar gives K of about 0.01. This value is about 20–40 times smaller than observed in ultrasonic experiments (e.g., Eberhardt-Phillips et al., 1989). The only way to explain this strong pressure dependency of velocities is to assume that some portion of the overall porosity has aspect ratios much smaller than 0.2.

Squirt flow in the presence of intermediate porosity

If the rock contains compliant, equant and intermediate porosity, two types of the squirt-flow will occur: (1) between compliant and stiff pores (equant plus intermediate) and (2) between intermediate and equant pores. The frequency dependence of the modified frame bulk modulus due to the flow between compliant and stiff pores is governed by equation 3 but with K_h replaced by the pressure-dependent modulus $K_{ds}(P) = 1/C_{ds}(P)$

$$\frac{1}{K_{\mathrm{mf}}(P,\omega)} = \frac{1}{K_{ds}(P)} + \frac{1}{\frac{1}{\frac{1}{K_d(P)} - \frac{1}{K_{ds}(P)}} + \frac{3i\omega\eta}{8\phi_c(P)\alpha_c^2}}. \quad (27)$$

The corresponding equation for the flow between intermediate and equant pores is

$$\frac{1}{K_{\mathrm{mf}}(P,\omega)} = \frac{1}{K_e} + \frac{1}{\frac{1}{\frac{1}{K_{ds}(P)} - \frac{1}{K_e}} + \frac{3i\omega\eta}{8\phi_m(P)\alpha_m^2}}. \quad (28)$$

Equations 27 and 28 can be combined to give a unified equation for the bulk modulus of the modified frame

$$\frac{1}{K_{\mathrm{mf}}(P,\omega)} = \frac{1}{K_e} + \frac{1}{\frac{1}{\frac{1}{K_{ds}(P)} - \frac{1}{K_e}} + \frac{3i\omega\eta}{8\phi_m(P)\alpha_m^2}} + \frac{1}{\frac{1}{\frac{1}{K_d(P)} - \frac{1}{K_{ds}}} + \frac{3i\omega\eta}{8\phi_c(P)\alpha_c^2}}. \quad (29)$$

Modulus K_{mf} can be used to obtain the bulk modulus of the fully saturated rock using Gassmann's or Biot's equations. The shear modulus is given by equations 4.

WORKFLOW

In this section, we outline the workflow that we applied to the ultrasonic velocities experimentally measured on dry sandstones to derive parameters of the pore microstructure and then to predict frequency dependent elastic properties of the saturated rock using these parameters. The workflow assumes that dry elastic properties (moduli and velocities) are independent of frequency (nondispersive).

1) Dry bulk and shear moduli K_d and μ_d at each confining pressure P_i are obtained from the ultrasonic measurements of the compressional and shear velocities V_P and V_S.
2) Parameters C_{ds0}, ϕ_{c0}, θ_c, and θ_s are obtained by the least-squares fitting of the dry compressibility $C_d(P_i) = 1/K_d(P_i)$ with equations 12.
3) Characteristic aspect ratio α_c of compliant pores is obtained using equation 13.
4) C_e is computed with CPA for spherical pores using K_g and μ_g, which can be obtained from the mineralogical composition of the rock, for instance, by Voigt-Reuss-Hill average (if elastic properties of composite materials are known) or by extrapolating of velocity-porosity regression to a zero-porosity limit. In this study, we did not know exact mineral composition of the rock and thus use the latter approach.
5) Values of $C_{ds}(P_i)$ for each pressure P_i are obtained by subtracting the exponential term $\theta_c C_{ds0}\phi_{c0}\exp(-\theta_c C_{ds0}P_i)$ from the dry compressibilities $C_d(P_i)$.
6) Constants ϕ_{m0} and ϕ_m are obtained by least-squares fitting of the values of $C_{ds}(P_i)$ with equations 19. Note that because the data only exist for pressures P_i much smaller than $(\theta_m C_e)^{-1}$, this fit is essentially linear.
7) The characteristic aspect ratio α_m of the intermediate pores is obtained using the expression for a dilute concentration of ellipsoidal cavities (cf. equations 13):

$$\theta_m = \frac{K_e(3K_e + 4\mu_e)}{\pi\alpha_m\mu_e(3K_e + \mu_e)}. \quad (30)$$

8) The compliant porosity $\phi_c(P)$ as given by equation 11 and the corresponding aspect ratio, α_c, are substituted into equations 27 and 4 to calculate the bulk and shear modified frame moduli $K_{\mathrm{mf}}(P,\omega)$ and $\mu_{\mathrm{mf}}(P,\omega)$ to account for the dynamic stiffness caused by the presence of the fluid in the grain contact area and pressure relaxation between compliant and stiff pores.
9) Likewise, intermediate porosity $\phi_m(P)$ given by equation 17 and the corresponding aspect ratio, α_m can be substituted into equations 28 and 4 to account for pressure relaxation between intermediate and equant pores.
10) The two models for the bulk modulus are combined using equation 25.
11) The frequency- and pressure-dependent bulk modulus $K_s(P,\omega)$ of the fully saturated rock is computed with the Gassmann equation 5, and together with the shear modulus $\mu_s(P,\omega) = \mu_{\mathrm{mf}}(P,\omega)$ is used to compute complex and fre-

quency- and pressure-dependent compressional and shear velocities $V_P(P,\omega) = \{[K_s + (4/3)\mu_s]/\rho\}^{1/2}$ and $V_S(P,\omega) = \{\mu_s/\rho\}^{1/2}$, where ρ is density of the saturated rock. The real part of these complex velocities defines the phase velocity of the corresponding waves, while the imaginary part defines attenuation.

DATA EXAMPLES

Pressure dependency of the ultrasonic velocities

The compressional and shear velocities predicted with the above workflow (from dry measurements) can be compared to laboratory measurements on wet samples. Most common and robust are time-of-flight measurements using a narrow-band ultrasonic pulse with a central frequency between 0.25 and 1 MHz. Such measurements effectively yield ultrasonic velocities in a narrow frequency band in a range of pressures between 0 and 50 MPa.

We illustrate the above workflow with ultrasonic measurements on dry and wet sandstones reported by Han et al. (1986). As the first example, we consider ultrasonic measurement data for a St. Peter sandstone sample, a typical reservoir rock with a porosity of about 20%. Figure 4 shows the decrease of the dry compressibility (calculated from compressional and shear ultrasonic velocities and density) with increasing pressure in the range 5–50 MPa (open circles). This decrease is well described by a combination of exponential and linear terms, equation 12, with the exponential term vanishing at about 20–25 MPa. The fitting using equation 12 gives $\theta_c = 4.2 \times 10^3$ which corresponds to the aspect ratio $\alpha_c = 0.15 \times 10^{-3}$. The fitting curve is shown in Figure 4 by the solid line. Note that the characteristic frequency f_c of the squirt dispersion as described by equations 3 and 4 is approximately given by

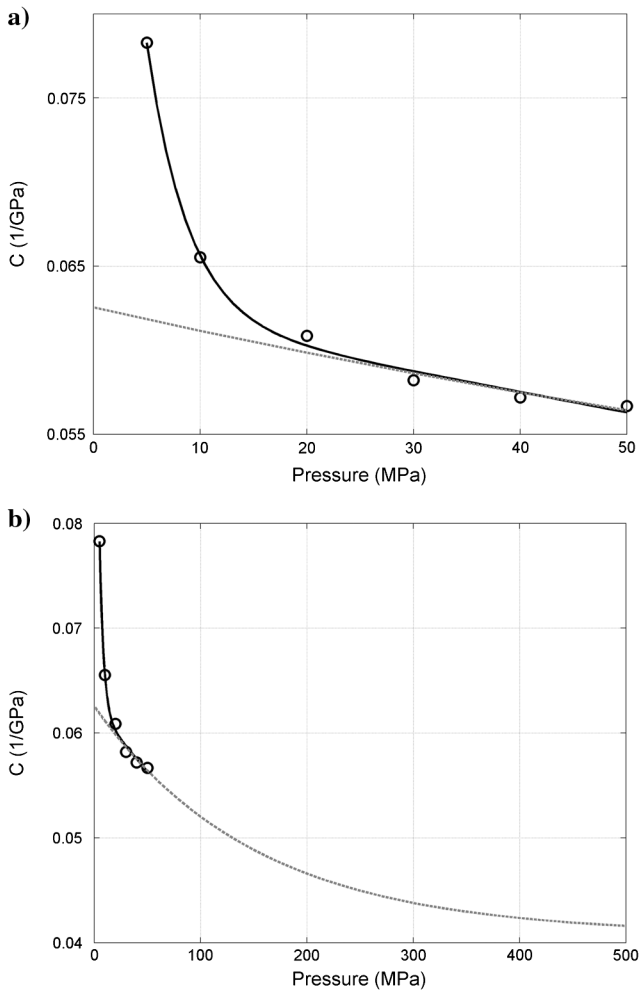

Figure 4. Compressibilities of a dry sample of St. Peter sandstone versus pressure: (a) Calculated from ultrasonic velocity measurements up to 50 MPa (open circles), (b) Predicted variations above 50 MPa due to closing of intermediate porosity (dashed line). Solid line shows the best fit of the experimental points with equations 12. Note the linear trend of compressibility against pressure after 25 MPa that implies the collapse of compliant pores at lower stresses.

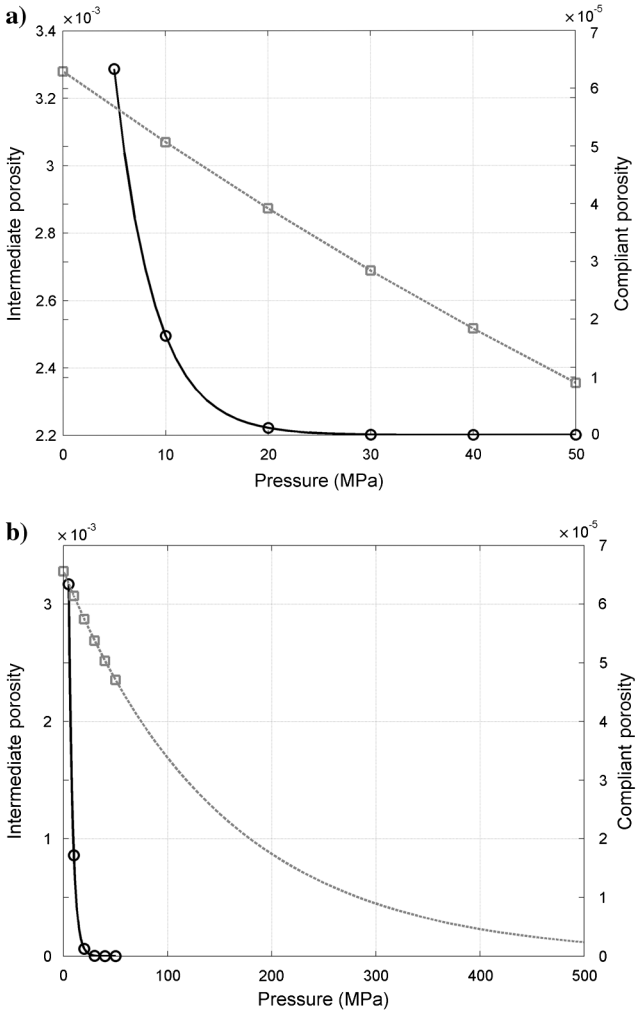

Figure 5. Compliant porosity ϕ_c (open circles and solid line) and intermediate porosity ϕ_m (open squares and dashed line) in a sample of St. Peter sandstone as a function of isotropic stress: (a) up to 50 MPa and (b) above 50 MPa. Note that intermediate porosity decreases almost linearly at low stresses. The magnitude of compliant porosity is approximately two orders decrease at low stresses and exhibits dramatic decay with the increase of pressure than one of intermediate porosity. Separate axes are used for these entities.

$$f_c \sim \frac{4\mu_h(3K_h+\mu_h)}{3(3K_h+4\mu_h)\eta}\alpha_c^3 \tag{31}$$

(Gurevich et al., 2010, equations 41–42). For the St. Peter sandstone sample, this gives $f_c \sim 50$ Hz. This frequency is in the seismic exploration range and well below the frequency of ultrasonic experiments. Thus, the dispersion at ultrasonic frequencies only can be explained by the squirt from the pores with a larger aspect ratio, that is, with intermediate porosity. Indeed, the aspect ratio of the intermediate porosity is $\alpha_m = 3.9\times10^{-3}$, which gives $f_c \sim 0.8\times10^6$ Hz, right within the typical range of ultrasonic measurements.

As can be seen in Figure 2, at the maximum stress of 50 MPa, the bulk modulus reaches 18 GPa, which is below the CPA estimate of $K_e = 23$ GPa. We explain this difference by the presence of the intermediate porosity. The dashed line in Figure 4b shows the projected pressure dependency of the dry compressibility in a broader pressure range, as predicted by the model with the intermediate porosity, equation 19. The pressure dependency of the corresponding compliant porosity ϕ_c (solid line) and intermediate porosity ϕ_m (dashed line) are shown in Figure 5a and 5b. Note the linear behavior of ϕ_m at pressures below 50 MPa.

The stress dependencies of the bulk and shear moduli of dry and wet St. Peter sandstone are shown in Figure 6a and 6b. In Figure 6a, circles and squares show measured values of the bulk modulus of the dry and saturated rock, respectively. Dotted and solid lines show

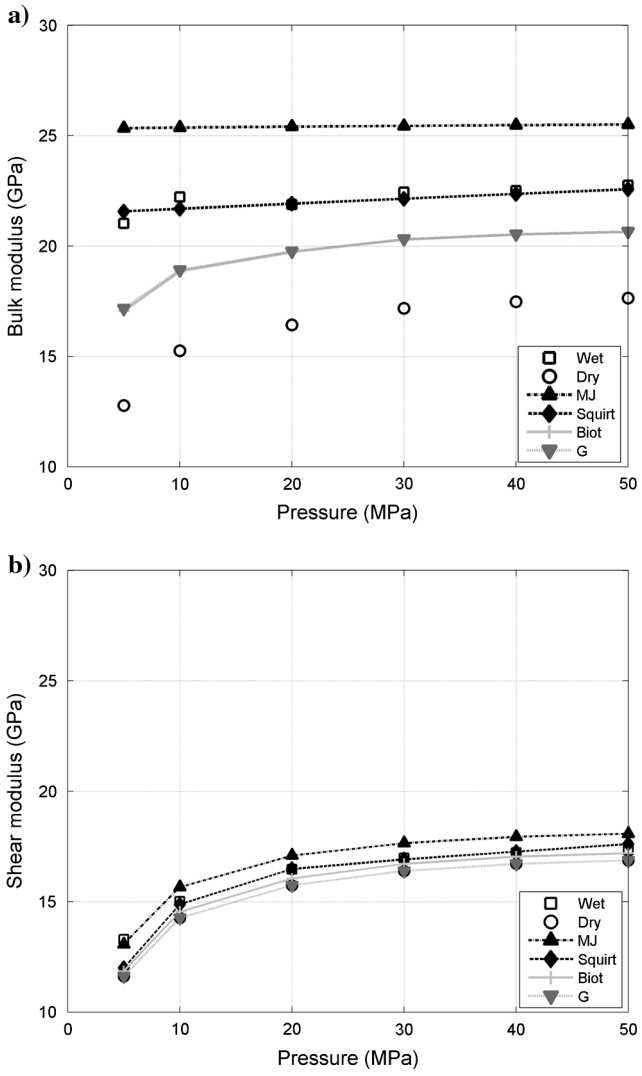

Figure 6. Saturated moduli the St. Peter sandstone predicted by a number of theories as a function of pressure: (a) bulk and (b) shear. Gassmann (invert triangles and dotted line) and Bio (cross and solid line) theories underestimate the measured bulk and shear moduli while Mavko and Jizba's model (triangles and dashed-and-dotted line) overestimates them. A good fit for both moduli is obtained with the newly developed squirt model (rhombs and dashed line). Dry and saturated moduli calculated from ultrasonic velocities are shown by open circles and squares, respectively.

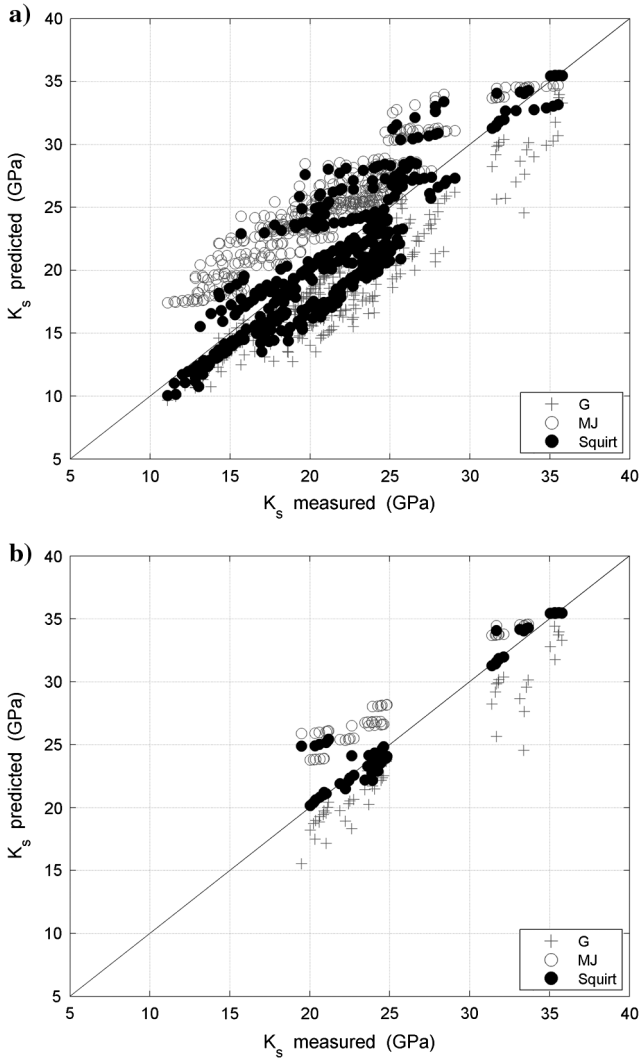

Figure 7. Predicted versus measured saturated bulk moduli for the pressure range from 5 to 50 MPa: (a) for all 66 sandstone samples and (b) for clean sandstones only (Han et al., 1986). Gassmann (crosses) predictions underestimate and Mavko and Jizba's model (open circles) overestimates the experimental data. The prediction of the newly developed squirt-flow dispersion model (solid circles) with the intermediate porosity is in a better agreement with the data, especially for the clean sandstones.

predictions of the Gassmann and Biot equations, respectively. The dash-dotted line shows the high-frequency limit as predicted using Mavko-Jizba (1991) equations. The dashed line is the prediction of the model of squirt between intermediate and equant pores, equations 28 and 6. The prediction of the squirt-flow dispersion model with the intermediate porosity is in an excellent agreement with the data. A similar observation can be made for the shear modulus (Figure 6b). It should be emphasized that the prediction is obtained from parameters extracted from dry measurements without any fitting to the measurements on saturated samples.

In Figure 7a and 7b the predicted saturated bulk modulus is plotted against the measurements for a number of sandstones. Crosses and open circles denote low-frequency (Gassmann) and high-frequency (Mavko-Jizba) limits, respectively, and solid circles are predictions of the newly developed squirt model. Figure 7a compares the results for all 66 sandstone samples from Han et al. (1986) and for the whole range of pressures 5–50 GPa. In most cases, Gassmann saturation without squirt underestimates the experimental data, while the Mavko-Jizba prediction overestimates the measurements. The saturated bulk moduli obtained with our workflow shows a somewhat better agreement with the measured moduli than either of the limits, but with a rather large scatter. The corresponding plot from the same data set but for clean sandstones only (nine samples) is shown in Figure 7b. The squirt model shows a very good agreement with the experiment for most, though not all, of the samples.

Prediction of dispersion and attenuation

Once the model parameters are extracted from dry rock measurements, the squirt model can be used to compute the elastic moduli, wave velocities and attenuation in a range of frequencies. Figure 8 shows predictions of the P and S velocities and attenuations, a reciprocal of a quality factor, Q, as functions of frequency and effective pressure for the St. Peter sandstone. At seismic frequencies, the velocities slowly increase with an increase of frequency until about 1 MHz (the value slightly varies with effective pressure). At this frequency, the squirt characteristic frequency for this water-saturated sample, a steep increase of the two velocities takes place. At frequencies higher than the characteristic frequency, velocities increase much more gradually.

At frequencies lower than the characteristic frequency, we expect a strong dependency of the velocity on pressure. At higher frequencies, the variation range of the velocities is much smaller. This observation can be easily understood if we recall that the effective pressure deforms the pore space and closes the thin cracks. At low stresses, these thin cracks substantially decrease the bulk moduli of the sandstone at low frequencies, at which the pressure induced by the passing wave can equilibrate. However, at ultrasonic frequencies and at the same stresses, the pore pressure has no time to equilibrate, making it much stiffer, while at higher stresses where the thin pores are partially closed, the difference in rock stiffness between low and high frequencies is smaller. In the ultimate case when all the thin pores are closed, the squirt flow would not cause any dispersion in the rock stiffness. The fact that, generally, measurements at ultrasonic frequencies in saturated sandstones deviate from the Gassmann predictions even at maximal effective stresses of 50–60 MPa indicates that thin pores still exist at those stresses.

Attenuation is also strongly frequency dependent. Figure 8b and 8d shows the predicted compressional dimensionless P and S wave attenuation factors ($1/Q$) for a range of frequencies. We observe that the attenuation increases with frequency until it reaches the maximum value at the squirt characteristic frequency. After that, the attenuation starts to decrease until 10^7 Hz, after the rate of the decrease changes (as discussed in Gurevich et al., 2010). The attenuation is slightly dependent on pressure, showing an inverse relation: the minimum pressure (blue) corresponds to a maximum attenuation. This is true for all frequencies; however, the variation with pressure is stronger at frequencies lower than the characteristic frequency.

As discussed earlier, the velocity dispersion at an ultrasonic frequency is consistent with the model of squirt flow between intermediate and equant pores. The squirt flow between compliant and stiff pores has a much lower characteristic frequency (50 Hz for St. Peter's sandstone) and thus may be important in the seismic frequency band. Figure 9a and 9b shows histograms of characteristic frequencies of the squirt between compliant and stiff pores (gray) and between intermediate and equant pores (black). Figure 9a is for all 66 samples and Figure 9b is for a subset consisting of clean sandstones only. We see that for most samples, the characteristic frequency of the squirt between compliant and stiff pores is in the seismic frequency band.

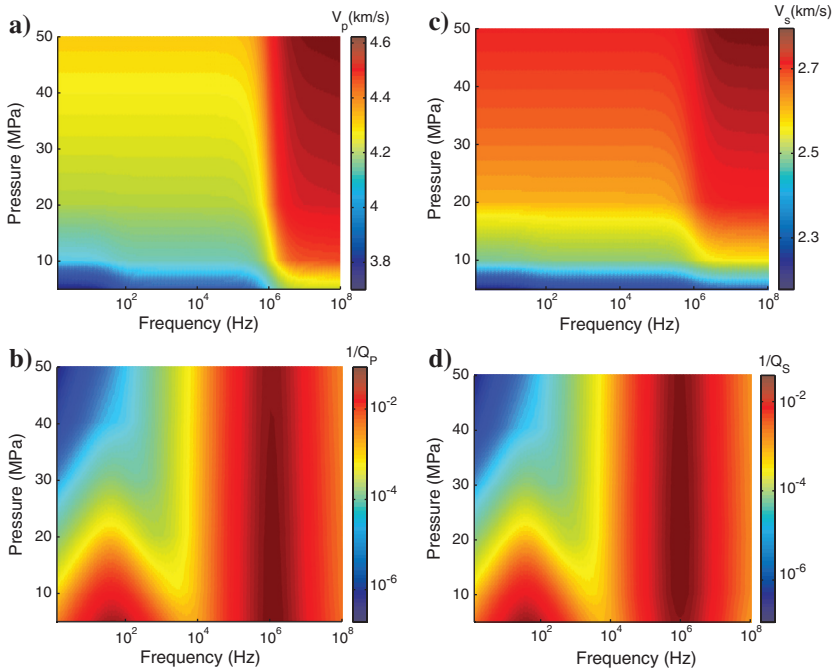

Figure 8. Dispersion and attenuation of compressional and shear velocity as a function of pressure and for the wide frequency range from seismic to ultrasonic: (a-b) dispersion and attenuation of V_P (c-d) dispersion and attenuation of V_S.

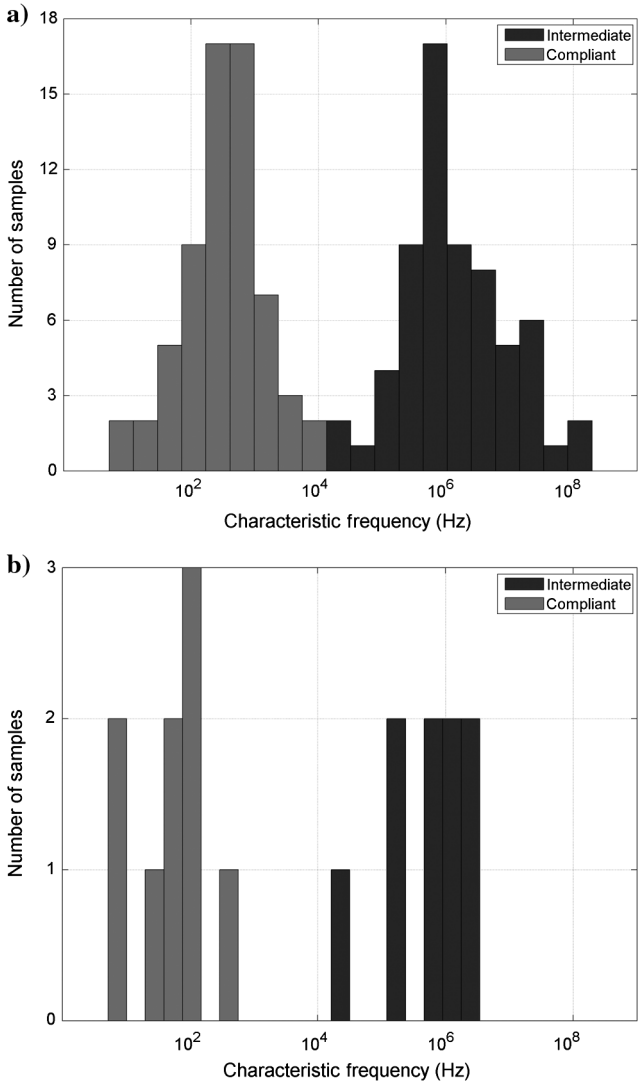

Figure 9. Histogram of characteristic frequencies of the squirt: (a) for all 66 samples; (b) subset of clean sandstones (Han et al., 1986). Characteristic frequencies of the squirt between compliant and stiff pores and between intermediate and equant pores are shown by grey and black, respectively.

DISCUSSION

The model presented here is based on the concept that the pore space in the rock can be divided into three distinct portions: compliant pores that close at effective pressures of up to 50 MPa, intermediate pores that close at much higher pressures (say, 200–2000 MPa), and equant pores with the aspect ratio of the order one, which do not deform noticeably for pressures up to 2000 MPa. We are not suggesting that the rock contains ellipsoidal pores with three distinct aspect ratios, rather, we suggest that this is the maximum information about the aspect ratio distribution that can be obtained from ultrasonic measurements on dry samples in the confining pressure range of up to 50 MPa. This is not the only model consistent with these measurements. Other models (such as those based on the power-law pressure dependency) are possible but are beyond the scope of our study.

It also should be noted that when we talk about a characteristic aspect ratio, we mean a relatively narrow, unimodal but continuous distribution. An exponential pressure dependency of elastic moduli is consistent with the existence of compliant pores of a single aspect ratio, and, within measurement errors, with a unimodal distribution of aspect ratios. Because the pressure range of up to 50 MPa is barely sufficient to obtain one exponent, it is not possible to determine the width of this distribution. Thus, we use the model with one aspect ratio because it is the simplest model that fits the data and not because it gives a realistic description of the pore space. This applies even more obviously to the intermediate porosity, about which we have even less information. Again, we may have a spectrum of aspect ratios between 10^{-3}–2×10^{-1} but we describe it by a single aspect ratio because we lack information to describe it in any more detail. Measurements over a much broader pressure range are necessary to characterize the pore space properties in more detail.

In discussing the deformation of the intermediate porosity, it is important to stress that our projected pressure dependencies in the range of up to 500 and even 2000 MPa are purely conceptual. One implicit assumption is that the solid grain material at all these pressures remains linearly elastic. This may not be the case, and indeed grains may even crush at these pressures (e.g., Zhang et al., 1990; Wong et al., 1997; Fortin et al., 2007). However, this will not affect our predictions because the real behavior at these high pressures is not explicitly used. Instead, we only use geometrical parameters of the pore space inferred from such hypothetical behavior, which is, in turn, inferred from the pressure dependency at pressures below 50 MPa, where the grains are linearly elastic.

We have analyzed the prediction of our squirt model for a large number of sandstones. To our knowledge, this has not been done before for any squirt model. Our results show that the model gives a reasonable agreement with the measurements for clean sandstones, but much less convincing agreement for shaley sandstones. This is understandable, because presence of clay may cause nonmechanical interactions between solid and fluid, which are not adequately described by any poroelasticity models. In addition, clays have a complex pore structure which may not be even roughly described by our simple models. Further studies are necessary to analyze whether the model works at least at modest clay content, and for other rocks.

Our analysis is based solely on measurements of pressure dependency of ultrasonic velocities of dry and wet sandstones. It is highly desirable to compare our predictions with experiments in a much broader frequency range, such as forced-oscillation quasi-static measurements (e.g., Batzle et al., 2006; Adelinet et al., 2010; Mikhaltsevitch et al., 2011). These novel measurements have a potential to substantially improve our understanding of dispersion and attenuation. However, these measurements are still in their infancy and require further analysis and calibration. We plan to analyze these measurements and compare the results with our predictions in a future study.

Apart from stress dependency of elastic properties of rock, other sources of data can give information on the rock pore system. Thin section data in 2D give information about the pore aspect ratio distribution(s). Three-dimensional microtomographic images can be used to obtain comprehensive information about intermediate and stiff porosity; however compliant pores cannot yet be resolved with current CT scanners (V. Shulakova, personal communication,

2011). Capillary pressure data can also be used to get information about pore throat distributions (unimodal or bimodal) and can further help constraining model assumptions. The proposed workflow should be further tested on a data set for which key model parameters such as grain elastic properties and pore space heterogeneity are measurable from core.

CONCLUSIONS

Modeling of dispersion and attenuation of elastic waves in fluid-saturated rocks due to the squirt flow requires the knowledge of a number of geometrical parameters of the pore space, in particular, the characteristic aspect ratio of the pores. These parameters are usually inferred by fitting the measurements on saturated rocks to the model predictions.

In this study, we have attempted to avoid such fitting. To this end, we have proposed to recover the geometrical parameters of the pore space from the pressure dependency of elastic moduli on dry samples. Once such parameters are obtained, they are substituted into the squirt model to predict the elastic moduli and compressional and shear velocities for a fluid-saturated rock. The velocity predictions can be compared with the measurements on saturated rocks.

Our analysis shows that the pressure dependency of elastic rock properties (and their deviation from Gassmann's prediction) at ultrasonic frequencies is controlled by the squirt flow between equant pores (with aspect ratio of order one) and intermediate pores (with aspect ratios between 0.3×10^{-4}–0.03×10^{-4}). Such intermediate porosity is only expected to hypothetically close at pressures in the 200–2000 MPa range, and thus cannot be directly obtained from ultrasonic experiments performed at pressures below 50 MPa. However, the presence of the intermediate porosity is inferred from two facts, (1) the significant linear trend in the pressure dependency of elastic properties of the dry rock and (2) the significant difference between the bulk modulus of the dry rock computed for spherical pores only and the measured modulus at the maximum pressure available in ultrasonic experiments (50 MPa). Furthermore, the linear trend below 50 MPa and the projected modulus in the high-pressure limit are used to infer the magnitude of the intermediate porosity and its characteristic aspect ratio. Substituting these parameters into the squirt model, we have computed elastic moduli and velocities of the water-saturated rock and compared these predictions against laboratory measurements of these velocities. The agreement is very good for a number of clean sandstones, but much worse for a broad range of shaley sandstones. This is understandable because the presence of micro porous clays makes the rock texture more complicated and the stress dependence of the heterogeneous sand-clay mix is no longer adequately described through the poroelastic model with three porosity types.

Our predictions also showed that dispersion and attenuation caused by the squirt flow between compliant and stiff pores may occur in the seismic frequency band. Confirmation of this prediction requires laboratory measurements of elastic properties at these frequencies.

ACKNOWLEDGMENTS

The authors gratefully acknowledge financial support from the Australian Research Council (Discovery-Project DP1096232) and the sponsors of the Curtin Reservoir Geophysics Consortium (CRGC). Osni Bastos de Paula is grateful to Petrobras for Ph.D. support at Curtin University. Dina Makarynska was supported by the Australian Postgraduate Award and CSIRO scholarship. The authors also wish to thank Colin M. Sayers and Serge A. Shapiro for stimulating discussions.

REFERENCES

Adelinet, M., J. Fortin, Y. Gueguen, A. Schubnel, and L. Geoffroy, 2010, Frequency and fluid effects on elastic properties of basalt: Experimental investigations: Geophysical Research Letters, **37**, no. 2, L02303, 10.1029/2009GL041660.

Batzle, M. L., D.-H. Han, and R. Hofmann, 2006, Fluid mobility and frequency dependent seismic velocity: Direct measurements: Geophysics, **71**, no. 1, N1–N10, doi: 10.1190/1.2159053.

Berge, P. A., J. G. Berryman, and B. P. Bonner, 1993, Influence of microstructure on rock elastic properties: Geophysical Research Letters, **20**, no. 23, 2619–2622, doi: 10.1029/93GL03131.

Berge, P. A., B. P. Bonner, and J. G. Berryman, 1995, Ultrasonic velocity porosity relationships for sandstone analogs made from fused glass-beads: Geophysics, **60**, 108–119, doi: 10.1190/1.1443738.

Berryman, J. G., 1980, Long-wavelength propagation in composite elastic media — I. Spherical inclusions: Journal of the Acoustical Society of America, **68**, 1809–1831, doi: 10.1121/1.385171.

Biot, M. A., 1962, Mechanics of deformation and acoustic propagation in porous media: Journal of Applied Physics, **33**, 1482–1498, doi: 10.1063/1.1728759.

Carcione, J., and B. Gurevich, 2011, Differential form and numerical implementation of Biot's poroelasticity equations with squirt dissipation: Geophysics, **76**, no. 6, 55–64, doi: 10.1190/geo2010-0169.1.

Chapman, M., S. V. Zatsepin, and S. Crampin, 2002, Derivation of a microstructural poroelastic model: Geophysical Journal International, **151**, 427–451, doi: 10.1046/j.1365-246X.2002.01769.x.

Christensen, R. M., 2005, Mechanics of composite materials: Dover Publications.

Cleary, M. P., I. W. Chen, and S. M. Lee, 1980, Self-consistent techniques for heterogeneous media: Journal of the Engineering Mechanics Division, ASCE, **106**, 5, 861–887.

Dvorkin, J., G. Mavko, and A. Nur, 1995, Squirt flow in fully saturated rocks: Geophysics, **60**, 97–107, doi: 10.1190/1.1443767.

Eberhart-Phillips, D., D.-H. Han, and M. D. Zoback, 1989, Empirical relationships among seismic velocity, effective pressure, porosity and clay content in sandstone: Geophysics, **54**, 82–89, doi: 10.1190/1.1442580.

Fortin, J., Y. Guéguen, and A. Schubnel, 2007, Effects of pore collapse and grain crushing on ultrasonic velocities and V_p/V_s: Journal of Geophysical Research, **112**, B08208, doi: 10.1029/2005JB004005.

Gassmann, F., 1951, Über die elastizität poröser medien (elasticity of porous media): Vierteljahrsschrift der Naturforschenden Gesellschaft in Zürich, **96**, 1–23.

Gurevich, B., D. Makarynska, O. B. de Paula, and M. Pervukhina, 2010, A simple model for squirt-flow dispersion and attenuation in fluid-saturated granular rocks: Geophysics, **75**, no. 6, 109–120, doi: 10.1190/1.3509782.

Han, D-H., A. Nur, and D. Morgan, 1986, Effects of velocity and clay content on wave velocities in sandstones: Geophysics, **51**, 2093–2010, doi: 10.1190/1.1442062.

Jones, T. D., 1986, Pore fluids and frequency dependent wave propagation in rocks: Geophysics, **51**, 1939–1953, doi: 10.1190/1.1442050.

Kuster, G. T., and M. N. Toksöz, 1974, Velocity and attenuation of seismic waves in two phase media: Geophysics, **39**, 587–618, doi: 10.1190/1.1440450.

Mavko, G., and D. Jizba, 1991, Estimating grain-scale fluid effects on velocity dispersion in rocks: Geophysics, **56**, 1940-1949, doi: 10.1190/1.1443005.

Mavko, G., and A. Nur, 1975, Melt squirt in the aesthenosphere: Journal of Geophysical Research, **80**, 1444–1448, doi: 10.1029/JB080i011p01444.

Mavko, G., and A. Nur, 1979, Wave attenuation in partially saturated rocks: Geophysics, **44**, 161–178, doi: 10.1190/1.1440958.

Mikhaltsevitch, V., M. Lebedev, and B. Gurevich, 2011, A low-frequency laboratory apparatus for measuring elastic and anelastic properties of rocks: 81st Annual International Meeting, SEG, Expanded Abstracts, 2256–2260.

Murphy, W. F., III, K. W. Winkler, and R. L. Kleinberg, 1986, Acoustic relaxation in sedimentary rocks: Dependence on grain contacts and fluid saturation: Geophysics, **51**, 757–766, doi: 10.1190/1.1442128.

Norris, A. N., 1985, A differential scheme for the effective moduli of composites: Mechanics of Materials, **4**, no. 1, 1–16, doi: 10.1016/0167-6636(85)90002-X.

O'Connell, R., and B. Budiansky, 1977, Viscoelastic properties of fluid-saturated cracked solids: Journal of Geophysical Research, **82**, 5719–5735, doi: 10.1029/JB082i036p05719.

Palmer, I. D., and M. L. Traviolia, 1980, Attenuation by squirt flow in undersaturated gas sands: Geophysics, **45**, 1780–1792, doi: 10.1190/1.1441065.

Pervukhina, M., B. Gurevich, D. N. Dewhurst, and A. F. Siggins, 2010, Experimental verification of the physical nature of velocity-stress relationship for isotropic porous rocks: Geophysical Journal International, **181**, 1473–1479, doi: 10.1190/1.3255251.

Shapiro, S. A., 2003, Elastic piezosensitivity of porous and fractured rocks: Geophysics, **68**, 482–486, doi: 10.1190/1.1567216.

Takei, Y., 2002, Effect of pore geometry on V_P/V_S from equilibrium geometry to crack: Journal of Geophysical Research, **107**, B2, 2043, doi: 10.1029/2001JB000522.

Thomsen, L., 1995, Elastic anisotropy due to aligned cracks in porous rock: Geophysical Prospecting, **43**, 805–829, doi: 10.1111/gpr.1995.43.issue-6.

Tod, S. R., 2002, The effects of stress and fluid pressure on the anisotropy of interconnected cracks: Geophysical Journal International, **149**, 149–156, doi: 10.1046/j.1365-246X.2002.01626.x.

Vernik, L., and J. Hammam, 2009, Stress sensitivity of sandstones and 4D applications: The Leading Edge, **28**, 90–93, doi: 10.1190/1.3064152.

Walsh, J. B., 1965, The effect of cracks on the compressibility of rock: Journal of Geophysical Research, **70**, 381–389, doi: 10.1029/JZ070i002p00381.

Wong, T.-F., C. David, and W. Zhu, 1997, The transition from brittle faulting to cataclastic flow in porous sandstone: Mechanical deformation: Journal of Geophysical Research, **102**, no. B2, 3009–3025, doi: 10.1029/96JB03281.

Zhang, J., T.-F. Wong, and D. M. Davis, 1990, Micromechanics of pressure-induced grain crushing in porous rocks: Journal of Geophysical Research, **95**, no. B1, 341–352, doi: 10.1029/JB095iB01p00341.

Zhang, J. J., T. F. Wong, and D. M. Davis, 1990, Micromechanics of pressure-induced grain crushing in porous rocks: Journal of Geophysical Research, **95**, no. B1, 341–352, doi: 10.1029/JB095iB01p00341.

Zimmerman, R. W., 1991, Compressibility of sandstones: Elsevier.